Provided for non-commercial research and education use.
Not for reproduction, distribution or commercial use.

This article appeared in a journal published by Elsevier. The attached copy is furnished to the author for internal non-commercial research and education use, including for instruction at the authors institution and sharing with colleagues.

Other uses, including reproduction and distribution, or selling or licensing copies, or posting to personal, institutional or third party websites are prohibited.

In most cases authors are permitted to post their version of the article (e.g. in Word or Tex form) to their personal website or institutional repository. Authors requiring further information regarding Elsevier's archiving and manuscript policies are encouraged to visit:

http://www.elsevier.com/copyright

Author's personal copy

Applied Surface Science 257 (2011) 7025–7029

Contents lists available at ScienceDirect

Applied Surface Science

journal homepage: www.elsevier.com/locate/apsusc

Structural and electrical properties of evaporated Fe thin films

M. Mebarki [a], A. Layadi [a,*], A. Guittoum [b], A. Benabbas [c], B. Ghebouli [a], M. Saad [b], N. Menni [d]

[a] Département de Physique, Université Ferhat Abbas, Sétif 19000, Algeria
[b] Centre de Recherche Nucléaire d'Alger (CRNA), Alger 16000, Algeria
[c] Laboratoire L.I.M.E, Université de Jijel, Jijel 18000, Algeria
[d] Faculté des Sciences de l'Ingénieur, Université Ferhat Abbas, Sétif 19000, Algeria

ARTICLE INFO

Article history:
Received 8 November 2010
Received in revised form 24 February 2011
Accepted 24 February 2011
Available online 13 April 2011

Keywords:
Thin films
Fe
Structure
XRD
RBS
SEM
Electrical resistivity

ABSTRACT

Series of Fe thin films have been prepared by thermal evaporation onto glass and Si(1 0 0) substrates. The Rutherford backscattering (RBS), X-ray diffraction (XRD), Scanning electron microscopy (SEM) and the four point probe techniques have been used to investigate the structural and electrical properties of these Fe thin films as a function of the substrate, the Fe thickness t in the 76–431 nm range and the deposition rate. The Fe/Si samples have a $\langle 1\,1\,0\rangle$ for all thicknesses, whereas the Fe/glass grows with a strong $\langle 1\,0\,0\rangle$ texture; as t increases (>100 nm), the preferred orientation changes to $\langle 1\,1\,0\rangle$. The compressive stress in Fe/Si remains constant over the whole thickness range and is greater than the one in Fe/glass which is relieved when $t > 100$ nm. The grain size D values are between 9.2 and 30 nm. The Fe/glass films are more electrically resistive than the Fe/Si(1 0 0) ones. Diffusion at the grain boundary seems to be the predominant factor in the electrical resistivity ρ values with the reflection coefficient R greater in Fe/glass than in Fe/Si. For the same thickness (100 nm), the decrease of the deposition rate from 4.3 to 0.3 Å/s did not affect the texture and the reflection coefficient R but led to an increase in D and a decrease in the strain and in ρ for both Fe/glass and Fe/Si systems. On the other hand, keeping the same deposition rate (0.3 Å/s) and increasing the thickness t from 76 to 100 nm induced different changes in the two systems.
© 2011 Elsevier B.V. All rights reserved.

1. Introduction

Fe and Fe based alloys are among the most studied systems in magnetism. For decades, Fe has been studied as thin film or as a part of a multilayer system [1–5]. The interest arises from the fact that these systems have been found to have a broad range of structural and magnetic properties which depend in part on the substrate or underlayer, the thickness, the method and the conditions of deposition such as substrate temperature, deposition rate, pressure and power. The effect of substrates and underlayers on the physical properties of Fe thin films has been thoroughly investigated; Fe thin films were grown on different substrates [6–14] and by different methods [15–17].

In the present work, we have investigated the structural and electrical properties of evaporated Fe thin films as a function of the substrate (glass and Si), the thickness (in the 76–431 nm range) and the deposition rate. We have attempted to separate the effect of the substrate, the thickness and the deposition rates on these physical properties.

2. Experimental methods

The Fe thin films were deposited by thermal evaporation onto glass and Si(1 0 0) substrates from a 99.99% purified Fe powder. Each series [Fe/glass and Fe/Si] consists of samples with different thicknesses. Pressure was about 3.8×10^{-7} mbar before evaporation; during deposition, it rises to 10^{-6} mbar. Different deposition rates were used. Rutherford backscattering spectroscopy (RBS) was used to probe the Fe/substrate interface and to measure the Fe thickness, which ranges from 76 to 413 nm. The RBS experiments were done using 2 MeV He^{+} ions delivered by a 3.75 MV Van de Graaf accelerator, the backscattering angle is equal to 20°. The structural properties (texture, lattice constant and grain sizes) were inferred from the X-ray diffraction (XRD) method working in the θ–2θ mode with a wavelength $\lambda = 1.54$ Å. Surface images were obtained by means of the scanning electron microscopy (SEM). The electrical resistivity ρ of the samples was obtained from the sheet resistance, which was measured by the four point method.

3. Results and discussions

Examples of RBS spectra are shown in Fig. 1a for Fe/glass sample with Fe thickness $t = 160$ nm and in Fig. 1b for Fe/Si one with $t = 105$ nm. The simulated spectra (solid lines) are obtained using

* Corresponding author.
E-mail address: A_Layadi@yahoo.fr (A. Layadi).

0169-4332/$ – see front matter © 2011 Elsevier B.V. All rights reserved.
doi:10.1016/j.apsusc.2011.02.114

Author's personal copy

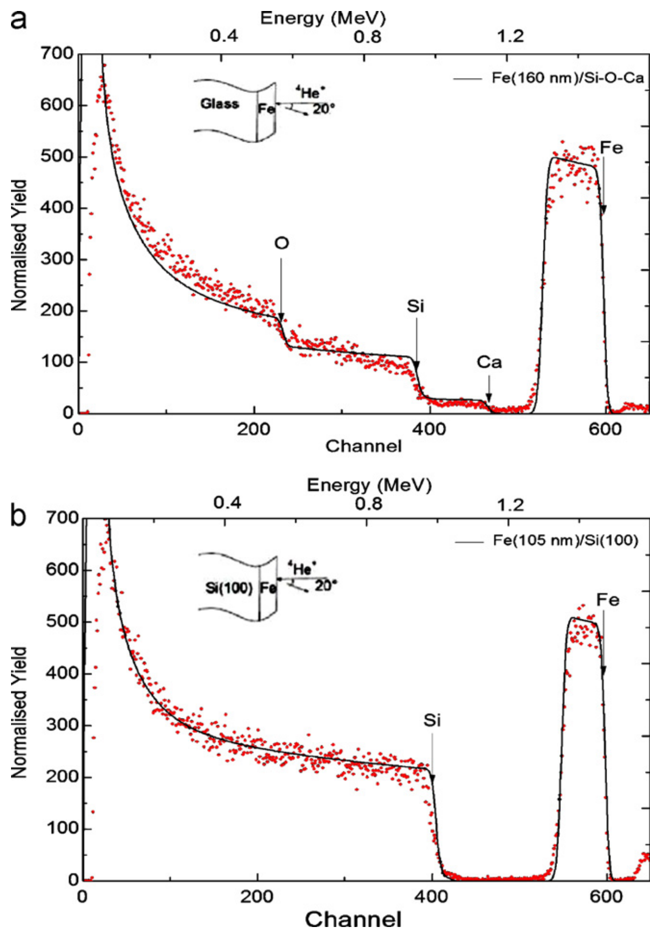

Fig. 1. RBS spectra for (a) Fe/glass with $t = 160$ nm, (b) Fe/Si(1 0 0) with $t = 105$ nm. The points are experimental data; the solid line is the simulated spectra.

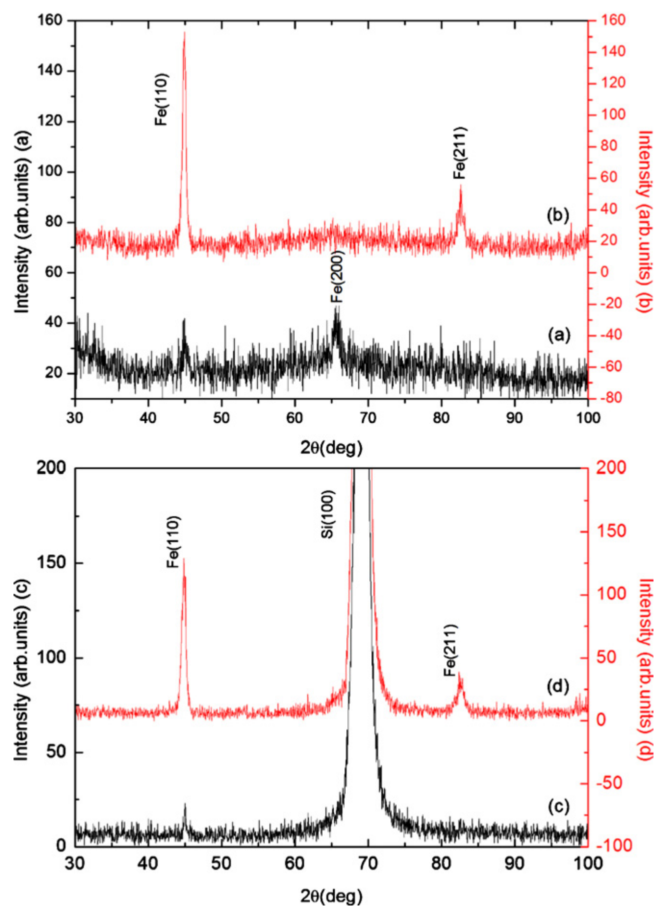

Fig. 2. X-ray diffraction spectra for Fe/glass (a) $t = 76$ nm, (b) $t = 431$ nm and Fe/Si(1 0 0) (c) $t = 76$ nm, (d) $t = 431$ nm.

the well-known SIMNRA code. The contributions of different elements of the film and the substrates are indicated in figure. In Fig. 1a, we found that the glass substrate consists of not only Si and O but also Ca; the inclusion of all these elements was necessary to obtain a good fit. In Fig. 1b, a good fit was achieved using Si and Fe elements. Such an experiment was carried out to probe the substrate-film interface and to measure the film thickness. We can see, in Fig. 1, that the different peaks are well separated, indicating that there is no interdiffusion at the interface between Fe and the substrates. From the fit of the experimental spectra and the simulated curves, we have inferred the film thickness. The Fe thicknesses are 76, 99, 105, 160 and 431 nm, with an error estimated to be less than 5%. The deposition rate ranges from 0.3 to 4.3 Å/s for the first four samples; the last one was grown with relatively higher deposition rate (13.7 Å/s).

Examples of X-ray diffraction spectra are shown in Fig. 2, for Fe/glass (Fig. 2a) and Fe/Si (1 0 0) (Fig. 2b) samples. For all Fe on glass samples, we observe a peak at $2\theta = 44.8°$ which has been identified as the (1 1 0) peak of the body centered cubic (bcc) Fe. For the thinnest sample (76 nm), a second peak appeared at $2\theta = 65.6°$ corresponding to the (2 0 0) peak while for the thickest one (431 nm), a peak at $2\theta = 82.7°$ can be seen and is assigned to the (2 1 1) peak. For the Fe on Si (Fig. 2b), besides the peak at $2\theta = 68.9°$ which corresponds to the (1 0 0) of the single crystal Si substrate, we observe for all samples a peak at $2\theta = 44.8°$ [the (1 0 0) peak of the bcc Fe]. Also for the 431 nm thick sample, another peak at $2\theta = 82.7°$ can be seen [the (2 1 1) Fe peak].

We have computed the intensity ratios I_{200}/I_{110}, I_{211}/I_{110}, (I_{200}, I_{211} and I_{110} refer to the intensities of the (2 0 0), (2 1 1) and (1 1 0) diffraction peaks) in order to determine the texture of these films. Note that for randomly oriented grains (no texture, i.e. the powder), we have $I_{200}/I_{110} = 0.38$ and $I_{211}/I_{110} = 0.176$. For Fe/glass, we found $I_{200}/I_{110} = 1.26$ for the 76 nm thick sample, indicating a ⟨2 0 0⟩ texture, while for all the other samples the preferred orientation is along the ⟨1 1 0⟩ direction. For the Fe/Si system, the only strong peak appearing is the (1 1 0) indicating a strong ⟨1 1 0⟩ texture for all samples. Thus, the Fe/glass starts growing with a strong ⟨1 0 0⟩ texture for the thinner film (76 nm), then the texture changes from ⟨1 0 0⟩ to ⟨1 1 0⟩ as the Fe thickness increases; whereas for the Fe/Si, the texture is ⟨1 1 0⟩ for all samples.

It should be noted that this ⟨1 1 0⟩ texture in Fe/Si was observed by other authors, e.g. in ion-beam mixing Fe/Si [18], in Fe/Si multilayer grown by ion-beam sputtering [19] and on a 30 nm thick RF sputtered Fe on Si(1 0 0) [20]. This ⟨1 1 0⟩ texture was also noted in Fe deposited on other substrates, e.g. on sapphire [21] and on V_2O_3 [22]. The ⟨1 0 0⟩ texture observed in the 76 nm thick Fe/glass has also been reported for Fe thin films, for example, in Fe/Ir(0 0 1) [23], in molecular-beam epitaxially deposited Fe on Cr [16], and in Fe/Au [24]. It is also interesting to note that the change of texture, such as the one we observed in Fe/glass as the thickness increases, was noted in other works but for different conditions. Indeed, in 15 nm DC magnetron sputtered Fe/glass films, the (1 1 0) texture was observed for substrate temperatures T_S less than 400 °C and changed to (0 0 2) for $T_S = 500$ °C [25]; the same authors reported that a change from (1 1 0) to (0 0 2) textures occurs after an annealing at 600 °C [25]. Also, a ⟨1 1 0⟩ texture was observed in evaporated Fe/glass with thickness less than 100 nm and for a low deposition rate (0.16 Å/s) and this texture changed to ⟨2 1 1⟩ as the thickness increased beyond 100 nm [26]. The change seems to occur

Author's personal copy

Table 1
Texture, out-of-plane strain ε, grain size D, sheet resistance $R_{\square}$, electrical resistivity ρ and reflexion coefficient R for Fe/glass and Fe/Si(1 0 0) for different Fe thicknesses, t. [For a fixed thickness (about 100 nm) and different deposition rates (4.3 Å/s and 0.3 Å/s) compare lines 2 and 3 for each system, and for a fixed deposition rate (0.3 Å/s) and different thicknesses (76 and 100 nm), compare lines 1 and 3 for each system.].

Thickness, t (nm)	Fe/Glass					
	Texture	ε (%)	D (nm)	$R_{\square}$ (Ω)	ρ (μΩ cm)	R
76	⟨1 0 0⟩	+0.14	9	3.92	30	0.40
99	⟨1 1 0⟩	+0.14	15	5.48	54	0.73
105	⟨1 1 0⟩	−0.10	30	3.08	32	0.72
160	⟨1 1 0⟩	−0.10	11	2.38	38	0.56
431	⟨1 1 0⟩	−0.10	22	0.97	42	0.73
Thickness, t (nm)	Fe/Si(1 0 0)					
	Texture	ε (%)	D (nm)	$R_{\square}$ (Ω)	ρ (μΩ cm)	R
76	⟨1 1 0⟩	−0.42	18	2.72	21	0.43
99	⟨1 1 0⟩	−0.73	11	3.64	36	0.54
105	⟨1 1 0⟩	−0.42	18	2.96	31	0.60
160	⟨1 1 0⟩	−0.42	14	0.51	8	/
431	⟨1 1 0⟩	−0.42	14	0.81	35	0.58

mainly in Fe/glass but not in the Fe/Si prepared under the same conditions.

From the lattice constants, derived from X-ray diffraction spectra, we have computed the out-of-plane strain defined as $\varepsilon = (a - a_{\text{bulk}})/a_{\text{bulk}}$, where a and a_{bulk} denote the measured and the bulk lattice parameter values. Values of ε are shown in Table 1. From Fe/glass, the strain ε is positive for $t < 100$ nm, i.e. the film is subjected to a tensile stress, as the thickness increases (>100 nm), ε becomes negative (compressive stress) and lower in absolute value, the stress seems to be relieved as the thickness increases. On the other hand, for the Fe/Si(1 0 0), the strain is always negative and is practically constant over all the considered thickness range. Moreover, for a given thickness, the strain in Fe/Si is greater (in absolute value) than the one computed in Fe/glass, i.e. there is more stress in Fe/Si than in Fe/glass samples.

The grain sizes have been derived from X-ray diffraction following the Scherrer method [27]. The grain size D for a grain with a particular orientation is given by:

$$D = \frac{k\lambda}{(\Delta\theta)\cos\theta} \quad (1)$$

where λ is the X-ray wavelength, k is a constant close to 1, θ the diffraction angle and $\Delta\theta$ is the width at half height of the peak corresponding to a particular orientation (here we used the (1 1 0) peak which is the most intense and corresponds to the texture of the films). The grain size values are shown in Table 1.

In Fig. 3, we show SEM surface images for Fe/glass (Fig. 3a and b) and for Fe/Si(1 0 0) (Fig. 3c and d) for the thinnest (76 nm) and thickest (431 nm) samples. For the 76 nm thick Fe/glass film, SEM images show smooth uniform surface (Fig. 3a) while for the thicker film (431 nm), small rounded shape droplets appear on the surface (Fig. 3b). For the Fe/Si samples, the SEM images reveal a uniform surface with very few relatively large droplets with circular shape for the thinner sample (76 nm), see Fig. 3c; for the thicker one (431 nm), a lot of smaller rounded shape droplets can be seen on the surface (Fig. 3d). The density of these droplets is greater in Fe/Si than in Fe/glass for the same thickness even though they were evaporated under the same conditions (at the same time) The formation of these droplets on the surface of the films seems to be due to the fact that the materials to be evaporated can be expelled from the target in a liquid state, this phenomenon has been reported in NiFe thin films [28,29]. Recall that these 431 nm thick samples were prepared with a high deposition rate (13.7 Å/s), we believe that this high deposition rate might be at the origin of the appearance of these droplets on the surface samples. Indeed, Chen et al. [30] observed the appearance of island-like grains on the surface of a Fe based alloy deposited on Si substrate. These island-like grains, similar to the ones we observe on our Fe thin films, appear only for high deposition rate (≥6 Å/s). Moreover, in our case we observe these island-like grains for higher deposition rate and also we noted that the number of these grains is greater in Fe/Si than in Fe/glass, the substrate does also affect this surface phenomenon. We will see in the following that the existence of these droplets in Fe may be responsible for the high electrical resistivity observed in these thicker samples.

The sheet resistance (called also square resistance) $R_{\square}$ is defined as $R_{\square} = \rho/t$, where ρ is the electrical resistivity and t the film thickness; $R_{\square}$ is measured in Ohms/square (Ω/□). The sheet resistance $R_{\square}$ values have been measured for all samples by the four point probe. In Fig. 4a, we show the variation of $R_{\square}$ with the film thickness t, for the Fe/glass and Fe/Si as indicated in figure. Besides the first point (76 nm), there is an overall decrease of $R_{\square}$ with thickness, with $R_{\square}$ [Fe/glass] higher than $R_{\square}$ [Fe/Si(1 0 0)] for a given thickness. Note that for the Fe/Si samples, the sheet resistance of the Si substrate without the Fe film was measured and found to be equal to 56.60 Ω. The sheet resistance values measured for the Fe/Si samples are between 0.5 and 3.6 Ω (see Table 1). These values are much lower than that of the Si substrate and thus can be taken as the Fe sheet resistance; this approximation falls within the uncertainties of the values. The electrical resistivity ρ was deduced from the sheet resistance $R_{\square}$. The variation of ρ with thickness is shown in Fig. 4b; the numbers appearing near the experimental points are the grain size values. We note that, for a given thickness, the ρ values in Fe/glass are always larger than the ones in Fe/Si(1 0 0). The origins of the variation of ρ with thickness are discussed in the following.

Several phenomena contribute to the electrical resistivity of thin films: the diffusion by the surface, the diffusion by the grain boundaries, the impurities, the defects and the magnetic disorder. In order to investigate the effect of some of these factors, we have studied the variation of ρ with the film thickness and the grain size, see Fig. 4b.

For Fe/glass, we observe that between t = 99 and 160 nm, ρ decreases (increases) with increasing (decreasing) grain size. This may indicate that diffusion by the grain boundaries is the important factor in the electrical resistivity of Fe/glass in this thickness range. The increase of ρ when t increases from 76 to 99 nm is not due to the surface diffusion (ρ should decrease with increasing thickness if that were the case) or to the diffusion by the grain boundaries (since the grain size increased ρ should decrease) or to a large impurity (since no phase other than Fe has been detected by X-ray Diffraction); this variation might be due to a small impurity (not detected by XRD) or to a defect present in the 160 nm thick sample.

For the Fe/Si samples, when t increases from 76 to 99 nm, the resistivity increases (see Fig. 4b) but this increase in ρ follows a decrease in grain size (from D = 18 nm to 11 nm) thus the variation in ρ in this thickness region is due to diffusion at the grain boundaries. Then between 99 and 160 nm, ρ decreases down to the Fe bulk value, this suggests that both diffusion at the surface and at the grain boundaries may play an important role in the resistivity values.

When t increases from 160 to 431 nm, we observe an increase in ρ, for both systems with the increase for the Fe/Si (330%) much greater than in the Fe/glass one (9.8%). This may be attributed to surface defects. Recall that the SEM images show droplets on the surface for the 431 nm thick sample with the density of droplets more important in Fe/Si than in the Fe/glass; that is why, we believe, the increase in ρ is more important in Fe/Si than in Fe/glass. Thus we may infer that these surface defects (appearance of droplets) are responsible for this increase in the electrical resistivity for these thicker films.

Author's personal copy

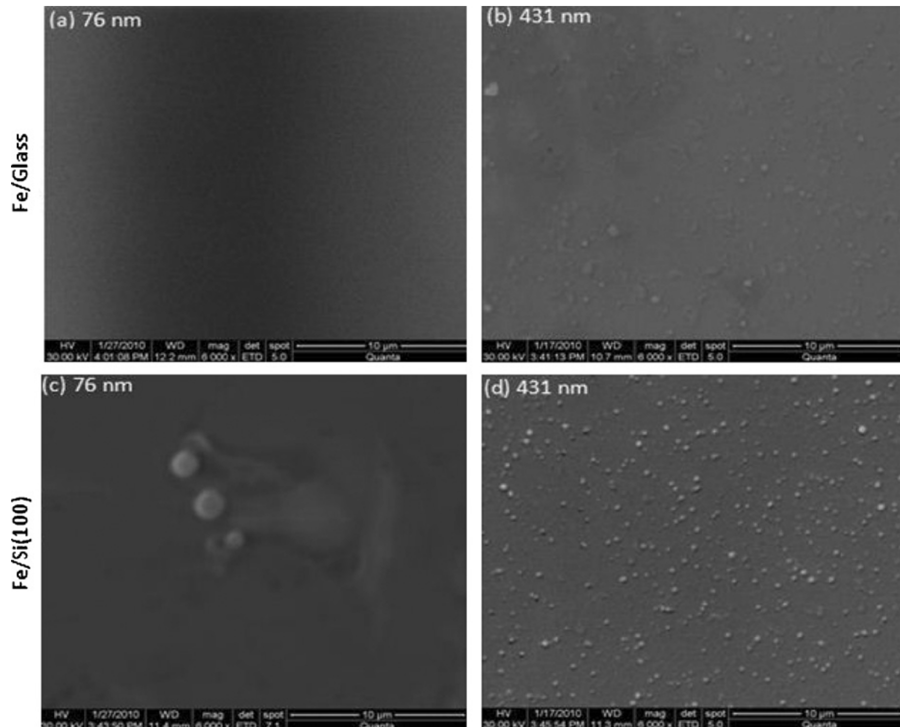

Fig. 3. SEM images for Fe/glass (a) t = 76 nm, (b) t = 431 nm and Fe/Si(1 0 0) (c) t = 76 nm, (d) t = 431 nm.

In order to determine the dominant factor, we have applied, to our experimental results, the Mayadas–Shatzkes model [31,32], which takes into account the diffusion at the grain boundaries. We found out that this model seems to describe well our experimental results confirming thus the first observation mentioned above. Recall that in this model, the resistivity ρ of the film is given by [32]:

$$\frac{\rho}{\rho_0} = \left[1 - \frac{3}{2}\alpha + 3\alpha^2 - 3\alpha^3 \ln\left(1 + \frac{1}{\alpha}\right)\right]^{-1} \quad (2)$$

where ρ_0 is the Fe bulk resistivity (ρ_0 = 9.72 $\mu\,\Omega$ cm) and

$$\alpha = \frac{\lambda}{D}\frac{R}{1-R} \quad (3)$$

Here λ is the bulk mean free path (for Fe, λ = 19.2 nm), D is the average grain size and R is the reflection coefficient, R takes values between 0 and 1; when R = 0, the diffusion at the grain boundaries is negligible while for R close to 1, it becomes very important. We have derived values of R using Eqs. (2) and (3). We found that besides the thinner samples (76 nm) where R is the same (0.41 ± 0.02) in both systems; for all other samples, R in Fe/glass (about 0.71) is always greater than the one observed in Fe/Si (0.58 ± 0.02). The R values depend not only on the substrate but also on the experimental conditions as can be seen by comparing the present results to those previously published on Fe thin films [33].

It appears from the above discussion that the different behaviors observed in these evaporated thin films may be due to the combination of the effects of the substrate, the thickness and the deposition rate. In the following we discuss the separate contribution of these three parameters on the physical properties of the Fe thin films. We will focus on the phenomena that can be attributed to each of the three parameters.

The effect of the substrate can be seen by comparing the Fe/glass and Fe/Si with the same thickness. Recall that for a given thickness, the Fe/glass and Fe/Si have been grown in the same run, i.e. under the same conditions, thus any differences in properties are due to the substrate. Some observations could clearly be attributed to the substrate. Indeed, for the thinner film (76 nm), the Fe/glass grows with the ⟨1 0 0⟩ texture while the Fe/Si has a strong ⟨1 1 0⟩ texture. The growth induced stress is lower in Fe/glass than Fe/Si(1 0 0). While the appearance of island-like grains or droplets in the surface of the thickest Fe deposited on both substrates is attributed to the high deposition rate as discussed above, the number of these droplets is higher in Fe/Si than in Fe/glass which is certainly an effect of the substrate. The effect of the substrate is more pronounced in the electrical properties: for the same thickness, the sheet resistance, the electrical resistivity and the reflection coefficients are always greater in Fe/glass than in Fe/Si, regardless of the thickness and the deposition rate values.

In order to distinguish between the effect of thickness and deposition rates, we note that the samples with nominal thicknesses equal to 99 and 105 nm have, within the measurement uncertainties, the same thickness (100 nm), the first one was grown at a rate of 4.3 Å/s while the second one at 0.3 Å/s. The differences in the physical the properties can then be attributed to the deposition rate.

In both systems, the decrease of the deposition rate from 4.3 to 0.3 Å/s with a fixed thickness (100 nm) did not affect the texture (the ⟨1 1 0⟩ texture), but led to a decrease in the strain and an increase in the grain size (compare lines 2 and 3 in Table 1). Also lower deposition rate produced a decrease in the sheet resistance and the electrical resistivity, while the reflection coefficient remains the same within the measurement uncertainties. Note however that the amounts of decrease for $R_{\square}$ and ρ are greater in Fe/glass than in Fe/Si, more than 40% in Fe/glass and less than 20% in Fe/Si.

Moreover, samples with thicknesses of 76 nm and 105 nm have been prepared with the same deposition rate (0.3 Å/s). With a fixed deposition rate (all other conditions being the same), we may assume that the different behaviors can be related to the thickness. The results pertaining to these two samples are shown also in Table 1 (compare lines 1 and 3 for each system). We observe then that for a fixed deposition rate, the increase of the thickness from 76 to 100 nm led to a change in the texture from ⟨1 0 0⟩ to ⟨1 1 0⟩,

Author's personal copy

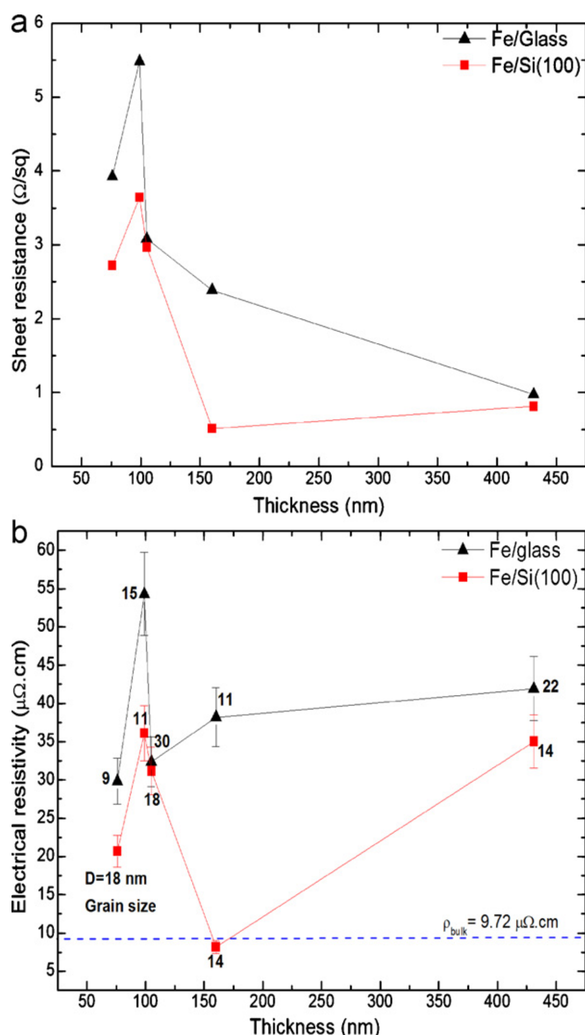

Fig. 4. The sheet resistance $R_\square$ (a) and the electrical resistivity (b) vs. Fe thickness for Fe/glass and Fe/Si(1 0 0). The values appearing near the experimental points in (b) are the corresponding grain sizes.

a decrease in the strain (with change of sign) and an increase in the grain size for the Fe/glass. However, for the Fe/Si, this increase in thickness did not change the texture (⟨1 1 0⟩) and did not affect neither ε (−0.42%) nor the grain size values (18 nm).

For the electrical properties, the increase in the thickness led to a decrease in the sheet resistance $R_\square$ (−21.4%), a small increase (8.5%) in the electrical resistivity and an increase in the reflection coefficient R (from 0.4 to 0.72) for the Fe/glass samples. While for the Fe/Si samples, increasing the Fe thickness (76 to 100 nm) led to an increase in $R_\square$ (8.8%), in ρ (50.7%) and in the reflection coefficient R (0.43 to 0.6). We can see that the effect of these preparation conditions on the physical properties does depend on the substrate for the Fe films.

4. Conclusion

We have experimentally observed that there are some differences and some similarities in the physical properties of Fe thin films when deposited on glass and on Si and when the Fe thickness, t, and the deposition rates are varied. The important behaviors are summarized as follow: (i) The Fe/glass start with the ⟨1 0 0⟩ texture; as t increases, this texture changes to ⟨1 1 0⟩; whereas for Fe/Si, the texture is ⟨1 1 0⟩ for all thicknesses. (ii) For Fe/glass, the strain ε is positive for $t < 100$ nm and becomes negative and smaller in absolute value for $t > 100$ nm, while for Fe/Si, the strain is negative and constant throughout the whole thickness range (76–431 nm); the stress in Fe/Si is greater than in Fe/glass. (iii) The Fe/glass samples are more electrically resistive than the Fe/Si ones, the diffusion at the grain boundaries seems to be the dominant factor in the electrical resistivity ρ with the reflexion coefficient R (Fe/glass) greater than R(Fe/Si). (iv) For a fixed thickness (100 nm), lowering the deposition rate led to a decrease in the stress and in ρ and an increase in the grain size D regardless of the substrate. (v) For a fixed deposition rate (0.3 Å/s), increasing t from 76 to 100 nm led to a decrease in ε and an increase in D for Fe/glass but did not affect ε and D for Fe/Si, and to a decrease in ρ for both systems. (vi) Finally, increasing the deposition rate seems to induce droplets on the film surface with greater density in Fe/Si than in Fe/glass. These surface defects seem to be responsible for the increase in ρ in these thick samples.

References

[1] B. Heinrich, S.T. Purcell, J.R. Dutcher, K.B. Urquhart, J.F. Cochran, A.S. Arrott, Phys. Rev. 38 (1988) 12879.
[2] A. Layadi, J.O. Artman, B.O. Hall, R.A. Hoffman, C.L. Jensen, D.J. Chakrabarti, D.A. Saunders, J. Appl. Phys. 64 (10) (1988) 5760–5762.
[3] Z. Celinski, K.B. Uquhart, B. Heinrich, J. Magn. Magn. Mater. 166 (1997) 6–12.
[4] S.M. Rezende, C. Chesman, M.A. Lucena, M.C. de Moura, A. Azevedo, F.M. de Aguir, J. Appl. Phys. 85 (1999) 5892.
[5] P.J. Sadashivaiah, T. Sankarappa, T. Sujatha, K. Santosh, R. Rawat, P Sarvanan, Bhatnagar A.K., Vacuum 85 (2010) 466.
[6] R. Naik, C. Kota, J.S. Payson, G.L. Dunifer, Phys. Rev. B 48 (1993) 1008.
[7] Y.B. Xu, E.T.M. Kernoham, D.J. Freeland, M. Tselepi, A. Ercole, J.A.C. Bland, J. Magn. Magn. Mater. 198–199 (1999) 181–190.
[8] F. D'Orazio, G. Gubbiotti, F. Lucari, E. Tassoni, J. Magn. Magn. Mat 242–245 (2002) 535–537.
[9] Y.V. Kundryavtsev, Y.P. Lee, J. Dubowik, B. Szymanski, J.Y. Rhee, Phys. Rev B65 (2002) 104417.
[10] M. Doi, B. Roldan Cuenya, W. Keune, T. Schmitte, A. Nefedov, H. Zabel, D. Spoddig, R. Meckenstock, J. Pelzl, J. Magn. Magn. Mater. 240 (2002) 407–409.
[11] C. Lallaizon, P. Schieffer, B. Lépine, A. Guivarc'h, F. Abel, C. Cohen, G. Feuillet, B. Daudin, F. Nguyen Van Dau., J. Cryst. Growth 240 (2002) 236–240.
[12] J.L. Costa-Kramer, J.L. Menéndez, A. Cebollada, F. Briones, D. Garcia, A. Hernando, J. Magn. Magn. Mater. 210 (2000) 341–348.
[13] M.A. Morales, H. Lassri, H.D. Fonseca Filho, A.M. Rossi, E. Baggio-Saitovitch, J. Magn. Magn. Mater. 256 (2003) 100–105.
[14] J. Swerts, K. Temst, N. Vandamme, C. Van Hasendonck, Y. Bruynseraede, J. Magn. Magn. Mater. 240 (2002) 380–382.
[15] M. Dreyer, C. Krafft, R.D. Gomez, IEEE Trans. Magn. 38 (2002) 2427.
[16] J. Pflaum, J. Pelzel, Z. Frait, P. Sturk, M. Marysko, P. Bodeker, K. Theis-Brohl, H. Zabel, J. Magn. Magn. Mater. 453 (1999) 198–199.
[17] T.C. Hufnagel, M.C. Kantzky, B.J. Daniels, B.M. Clemens, J. Appl. Phys. 85 (5) (1999) 2609–2616.
[18] M. Milosavljevic, G. Shao, N. Bibic, C.N. Mc Kinty, C. Jeyncs, K.P. Homewood, Appl. Phys. Lett. 79 (2001) 1438–1440.
[19] A. Chaiken, R.P. Michel, M.A. Wall, Phys. Rev. B53 (1996) 5518–5529.
[20] H.B. Nie, S.Y. Xu, C.K. Ong, Q. Zhan, D.X. Li, J.P. Wang, Thin Solid Films 440 (2003) 35–40.
[21] A. Ruediger, J. Yu, S. Zhang, A.D. Kent, S.S.P. Parkin, Phys. Rev. Lett. 80 (1998) 5639.
[22] B. Sass, S. Buschhorn, W. Flesch, D. Schmitz, P. Imperia, J. Magn. Magn. Mater. 303 (2006) 167–177.
[23] W. Schneider, S.L. Molodtsov, M. Richter, Th. Gantz, P. Engelmann, C. Laubschat, Phys. Rev. B57 (1998) 14930.
[24] I. Chiba, K. Himi, K. Saito, S. Mitani, K. Takanashi, K. Sato, H. Fujimori, J. Magn. Magn. Mater. 226–230 (2001) 1720–1721.
[25] S.H. He, C.L. Zha, B. Ma, Z.Z. Zhang, Q.Y. Jin, J. Magn. Magn. Mater. 310 (2007) 2658.
[26] B. Ghebouli, S.-M. Chérif, A. Layadi, B. Helifa, M. Boudissa, J. Magn. Magn. Mater. 312 (2007) 194–199.
[27] J.P. Eberhart, Analyse Structurale et Chimiques des Matériaux, Bordas, Paris, 1989.
[28] A.P. Caricato, M. Fernández, Z. Frait, D. Fraitova, S. Luby, A. Luches, E. Majkova, G. Majni, R. Malych, P. Mengucci, Appl. Phys. A 79 (2004) 1251–1254.
[29] A. Guittoum, A. Layadi, T. Kerdja, S. Lafane, S. Bouterfaia, Eur. Phys. J. Appl. Phys. 42 (2008) 235–239.
[30] S.L. Chen, W. Liu, Z.D. Zhang, J. Magn. Magn. Mater. 302 (2006) 306.
[31] A.F. Mayadas, M. Shatzkes, Phys. Rev. B1 (1970) 1382.
[32] A.I. Maarouf, B.L. Evans, J. Appl. Phys. 76 (1994) 1047–1054.
[33] B. Ghebouli, A. Layadi, A. Guittoum, L. Kerkache, M. Benkerri, A. Klimov, V. Preobrazhensky, P. Pernod, Eur. Phys. J. Appl. Phys. 48 (2009) 30503.